

Analysis and experimental investigation for collimator reflective mirror surface deformation adjustment

Chia-Yen Chan¹, Zhen-Ting You², Ting-Ming Huang¹, Yi-Cheng Chen^{2,*}, and Fong-Zhi Chen¹

¹*Instrument Technology Research Center, National Applied Research Laboratories, HsinChu, Taiwan*

²*Department of Mechanical Engineering, National Central University, Taoyuan City, Taiwan*

Article history:

Received 24 November 2015

Revised 18 March 2016

Accepted 29 March 2016

Keywords:

Collimator, Zernike polynomials, Finite element method, Supporting structure, Surface deformation, Wavefront aberration

Citation:

Chan, C. Y., Z. T. You, T. M. Huang, Y. C. Chen, and F. Z. Chen, 2017: Analysis and experimental investigation for collimator reflective mirror surface deformation adjustment. *Terr. Atmos. Ocean. Sci.*, 28, 167-176, doi: 10.3319/TAO.2016.03.29.01(EOF5)

ABSTRACT

Collimator design is essential for meeting the requirements of high-precision telescopes. The collimator diameter should be larger than that of the target for alignment. Special supporting structures are required to reduce the gravitational deformation and control the surface deformation induced by the mounting force when inspecting large-aperture primary mirrors (M1). A ZERODUR[®] mirror 620 mm in diameter for a collimator was analyzed using the finite element method to obtain the deformation induced by the supporting structures and adjustment mechanism. Zernike polynomials were also adopted to fit the optical surface and separate corresponding aberrations. The computed and measured wavefront aberration configurations for the collimator M1 were obtained complementally. The wavefront aberrations were adjusted using fine adjustment screws using 3D optical path differences map of the mirror surface. Through studies using different boundary conditions and inner ring support positions, it is concluded that the optical performance was excellent under a strong enough supporter. The best adjustment position was attained and applied to the actual collimator M1 to prove the correctness of the simulation results.

1. INTRODUCTION

With the resolution of space optical remote sensor getting higher, the aperture of primary mirrors (M1) has become increasingly larger with increasingly higher spaceborne optical remote sensing resolution. Collimator design is essential to satisfy the requirements of high-precision, large-aperture telescopes. The collimator diameter should be larger than that of the target for alignment without affecting the measurement results (Yang et al. 2005). Mirrors with larger apertures will increase the surface deformation and stress, resulting in image quality degradation. Therefore, suitable and rational support structures are required to reduce the deformation induced by gravity and control the surface deformation induced by the mounting force when mounting large-aperture optical mirrors.

There is no doubt that the location and the direction

of a mounting flexure are determined using kinematic principles and the ideal support location is in the plane through the mirror centroid and the lateral force should be vertical to the optical axis (Vukobratovich and Richard 1988; Yoder 2008; Chu et al. 2011; Kihm 2012). In mounting large mirrors, the common mount types are the V-type, radial, mercury tube, strap, and push-pull mounts for the horizontal optical axis. Ring, air bag, multiple-point supports, and metrology mounts are used for the vertical optical axis. Mechanical flotation, pneumatic/hydraulic, center-mounted, double-arch, bipod, and thin face sheet mounts are used for the optical axis with variable-orientation (Yoder 2005). A M1 support with an integral part of the active optics concept was designed by Beraud et al. (1995). The desired deformations were obtained by applying suitable force distributions through the axial support system. Axial loads are decoupled into a passive load distribution taken over by 150 hydraulic supports connected in three hydraulic sectors and an active load distribution. Each axial force actuator interfaces with

* Corresponding author
E-mail: ethan@cc.ncu.edu.tw

the mirror through a tripod assembly inducing local bending moments which dramatically reduce the high spatial frequency print-through. 0.5 μm root mean square (RMS) of mirror deformation can be achieved by modal corrections. The mirror surface deformation can also be improved by turning the 150 hydraulic active supports after obtaining the distortion corrections with a wavefront sensor located off-axis on the image surface. The static analyses for a flat reflector of interferometer in unassembled and assembled radial conditions, as well as horizontal and vertical placement under gravity load under, have been studied by Li et al. (2005) with the finite element method (FEM) and Zernike polynomial fittings. The calculated peak-to-valley (P-V) and RMS values were used to determine the rationality of the distortion and the structure of fixation. It was found that a rigid structure can improve the mirror deformation, but care must be made during mirror assembly to avoid imposing additional stress onto the mirror. A variety of support schemes and thermoelastic deformation for 460-mm diameter interferometer mirrors were studied by Xu et al. (2004) with the FEM. They found that the band support with 180° wrap angle and a dentiform rubber-lined strip is acceptable as the optimum and the influence of thermal effects is much greater than effects from mechanical forces. A mirror with a diameter of 620 mm with three comparative testing programs for vertical support was studied by Peng and Yuan (2009) with the finite element software and Zernike polynomials. By reducing the aberrations with great impact on the mirror, 0.025 λ ($\lambda = 632.8 \text{ nm}$) RMS of mirror deformation was achieved. Experiments for the three kinds of supports were carried out to verify that the entirely bound by strip is the best way for mounting the mirror. The strap mount for the horizontal optical axis is close to the ideal way to support the large mirrors, but astigmatism still occurs due to the combination of gravity and support positions (Peng et al. 2011).

However, center-mounted mounts are sometimes adopted to reduce thermal stress and surface deformation due to mirror free expansion and contraction during wide temperature variations. The surface figure changes in the meniscus M1, which is centrally supported and loaded by gravity (1g), were studied by Wu et al. (1996). The P-V and RMS values were used to determine whether the deformation is reasonable or not. The aberration composition of the mirror support was processed with Zernike polynomials. In this way, some approaches attempted to improve image quality were carried out and the rear mirror profile was optimized. A large-aperture mirror under gravity load was analyzed by Wu and Li (2011) with the FEM based on contact theory. They concluded that contact analysis is more accurate than linear analysis for large mirrors after several modules' computing and comparison between the calculated and test results.

Active optics is one of the important technologies used

for constructing high-precision, large-aperture telescopes. The performance of an active optics system needs to be analyzed theoretically in advance. Martin et al. (1998) studied an active support system and optimization of support forces for a 6.5 m M1. The mirror was figured to an accuracy of 26 nm RMS surface error, excluding certain flexible bending modes that will be controlled by support forces in the telescope. They mentioned that on mirror installation into its telescope support cell, an initial optimization of support forces is needed because of minor differences between the support used during fabrication and that in the telescope cell. The optimization was based on figure measurements made interferometrically in the vibration isolated test tower. Actuator influence functions were determined by finite element analysis (FEA) and verified by measurement. A 1.2 m active thin-mirror model with 36 axial supports and 3 lateral supports was built by Yao et al. (2010). In order to ensure the active optics system and select appropriate force actuators, the ability of the active optics system to duplicate the first 15 Zernike modes as well as the mirror deformations before and after active force corrections under gravitational loads were carried out through the FEA. Through the above analyses over the theoretical performance of the 1.2 m active thin-mirror, it was concluded that the support system is effective in maintaining the mirror surface and the maximum mirror stresses while fitting aberrations within the allowable stress of the glass material. Zhao et al. (2010) compared the differences in testing and manufacturing statuses between the M1 in space and on the ground. A support method for large-aperture M1 manufacturing and testing was released to carry out multiple discrete supports on the back of the mirror by controlling the support stress. The results indicate that the method could reduce the plane error of the M1 brought by its self-weight effectively when the mirror is being polished.

The aforementioned literature provided valuable information relevant to the self-weight induced phenomena (gravity effects) and adjustment mechanisms for large mirrors. However, most of the previous studies are limited to the impact of the inner support ring position related to the mirror centroid on the mirror deformation without taking account of the combined effect of the remaining supporting structure. Moreover, no quantitative optimum adjustment mechanism was found for the number and locations of adjustment screws.

A centrally supported ZERODUR® mirror, 620 mm in diameter for a collimator is computationally and experimentally investigated to obtain the deformation induced by the supporting structures and adjustment mechanism. The FEA and Zernike polynomials will be adopted to calculate and fit the optical surface and separate corresponding aberrations. The computed and measured wavefront aberration configurations will be complementally obtained. The optical performance will be investigated through studies under different boundary conditions and supporting positions for the

inner ring. The wavefront aberrations will be adjusted using the fine adjustment screws with the optical path differences (OPDs) 3D map of the mirror surface. The best adjustment position will be attained and applied to the actual collimator M1 to prove the correctness of the simulation results.

2. METHODOLOGY

2.1 Collimator and Adjustment Mechanism

The schematic of the collimator structure is shown in Fig. 1a. The collimator includes a parabolic (conic constant = -1) M1 with a diameter of 620 mm, a thickness of 100 mm, and a radius of curvature of 1219.2 mm, a main plate, a secondary mirror (M2), a supporter with ring support, four struts (Fig. 1b) and four fine adjustment screws (Fig. 1c). The ring support position is located on the M1 centroid, which is 35 mm from the reflective surface vertex, defined

as the system origin. Five other ring support positions are listed in Table 1 and will be taken into account in the calculations.

The cross arranged adjustment screws (Fig. 1c) are numbered A to D from the leftmost screw clockwise. Note that the four fine adjustment screws provide only linear motion on the mirror back. The various threads per inch (TPI) for the fine adjustment screws are listed in Table 2. In the present collimator the screws of TPI 80 are adopted and the corresponding forward displacements are also depicted in Table 2.

2.2 Experimental Measurement

The measurement system shown in Fig. 2 includes the collimator, an interferometer (Engineering Synthesis Design Incorporation Intellium H1000) mounted on an

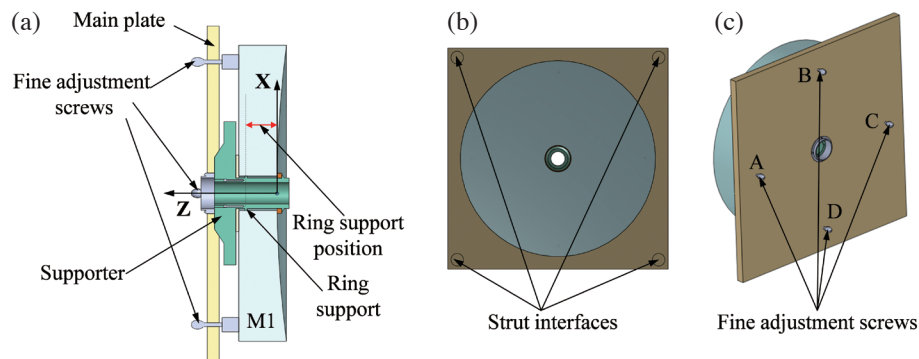


Fig. 1. (a) Schematic of the collimator structure, (b) front view, and (c) back view of the primary and main plate. (Color online only)

Table 1. Six ring support positions.

Position 1	15 mm
Position 2	25 mm
Position 3	35 mm (M1 centroid)
Position 4	40 mm
Position 5	50 mm
Position 6	65 mm

Table 2. Pitch and forward displacement for the fine adjustment screws.

TPI (Threads per Inch)	Pitch (mm revolution)	Rotation degree	Forward displacement (μm)
40	0.635	1°	0.88
80	0.318	2°	1.77
100	0.254	→ 3°	2.65
127	0.200	4°	3.53
200	0.127	5°	4.42
254	0.100	6°	5.30

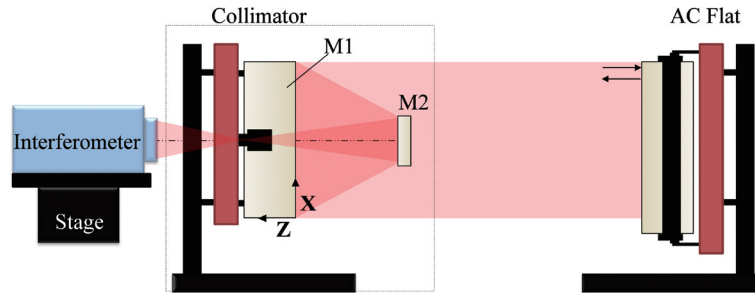


Fig. 2. Schematic of the experimental setup. (Color online only)

electronically controlled stage and a reference plate (AC flat). The laser beam is emitted from the interferometer through the central opening of M1 to M2, and then reflected back to M1 and afterwards to the AC flat. Similarly, the laser beam will be reflected to the interferometer on the same path to produce interference and the optical wavefront aberrations of the collimator system.

The internal structure of the adopted interferometer is a Fizeau interferometry arrangement, where the original laser beam and the beam reflected from the collimator and AC flat will pass through the spatial filter, optical system and non-polarizing, amplitude type beam splitter sequentially. The laser beam is then divided by the spectroscopic system and sent to three sets of independent cameras. The design making the interferometer take three simultaneous phase-shifting interferograms, shortening the time to take interferograms as well as reducing the impact of air turbulence and external shocks. Multiple interference pattern correlations can be calculated to obtain a wavefront map, which is the shape of the surface to be measured.

2.3 Finite Element Model and Physical Properties

The M1 is ZERODUR[®] glass ceramic (class 0), with a coefficient of thermal expansion near zero, density of 2530 kg m^{-3} , Young's modulus of 91 GPa and Poisson's ratio of 0.24 (Döhning et al. 2007). The fracture criterion of brittle ZERODUR[®] is determined by the maximum principle stress (MPS) of the mirror. The mirror blank is considered safe if the highest MPS is less than the ultimate strength divided by a safety factor of 1.5.

The corresponding unstructured grid system shown in Fig. 3 was constructed in the 3D computational domain for analysing the FEA results of the collimator M1. Solid186 is selected as the element type and there are three degrees of freedom at each node. Because of the uncertain constrained boundary conditions, five kinds of fixed support conditions numbered sequentially from A to E are described in Fig. 4. Based on the five restraint conditions, five chosen constrained boundary conditions ($u = 0$) numbered Cases 1 - 5 are listed in Table 3 for the preliminary simulations.

Conversely, other structures including the mirror body are free. For Case 3, the four strut interfaces, supporter back, and ring support are all fixed in the FEA. This also implies that the collimator structure becomes more rigid as the boundary conditions specified from Cases 1 - 5. In addition, the whole M1 is under self-weight deflection in the X direction. With the above well-posed boundary conditions, the model consists of 119841 nodes determined by the node convergence test. The results from the other simulation cases are then calculated at the same mesh density.

3. RESULTS AND DISCUSSION

3.1 Supporting and Restraint Conditions Effects on the Collimator M1 Surface Deformation

The mirror stress distributions for the ring support position = 35 mm for Cases 1 - 5 under self-weight are shown in Fig. 5. Due to the non-lightweight mirror, the mirror for the five cases leans forward (-Z direction). Although the maximum stresses for Cases 1 and 2 are smaller than those for Cases 3 - 5, the induced stress spreads to all of the mirror blank. For Cases 3 - 5, the stresses concentrate in the middle of the mirror blank around the ring support. Figure 6 depicts the corresponding surface deformations for the ring support position = 35 mm for Cases 1 - 5. It is found that the surface deformation pattern of Case 1 is different from those of other cases where the patterns are vertically symmetrical. The surface deformation pattern of Case 1 for ring support position = 35 mm is different from those for Cases 2 - 5.

Similarly, the surface OPD pattern of Case 1 for the ring support position = 35 mm is different from those of Cases 2 - 5 (Fig. 7). Case 1 with a P-V value of 0.425λ is dominated by astigmatism, and the coma patterns is shown clearly in Cases 2 - 5 whose P-V values are all below 0.1λ . It can be concluded that more constraint on the collimator reduces the P-V values and changes the optical aberration pattern from astigmatism into coma dominant patterns. This also indicates that Case 1 has weaker support. The relations between the astigmatism and coma in the X direction as well as the ring support positions for the five cases are shown in Figs. 8 and 9, respectively. The astigmatism (Fig. 8)

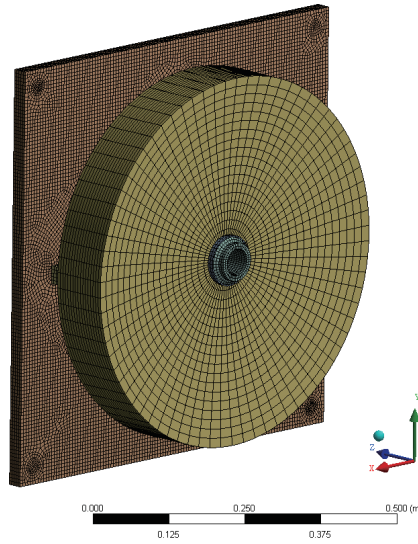


Fig. 3. Unstructured grid system for the collimator M1. (Color online only)

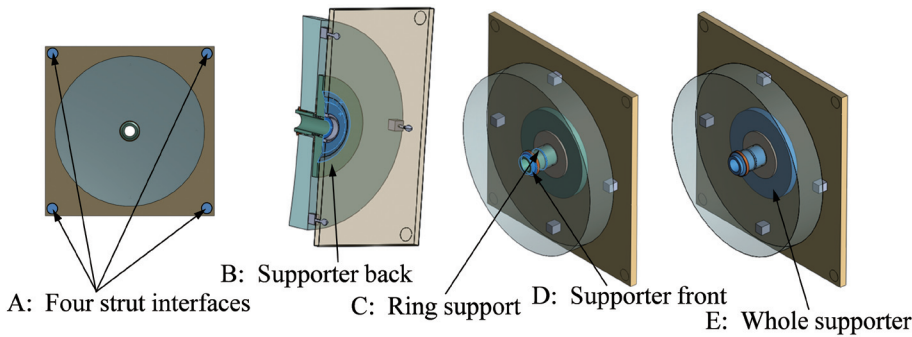


Fig. 4. Schematic of various fixed support conditions. (Color online only)

Table 3. Five fixed support conditions.

	Fixed support conditions
Case 1	A
Case 2	A + B
Case 3	A + B + C
Case 4	A + B + C + D
Case 5	A + E

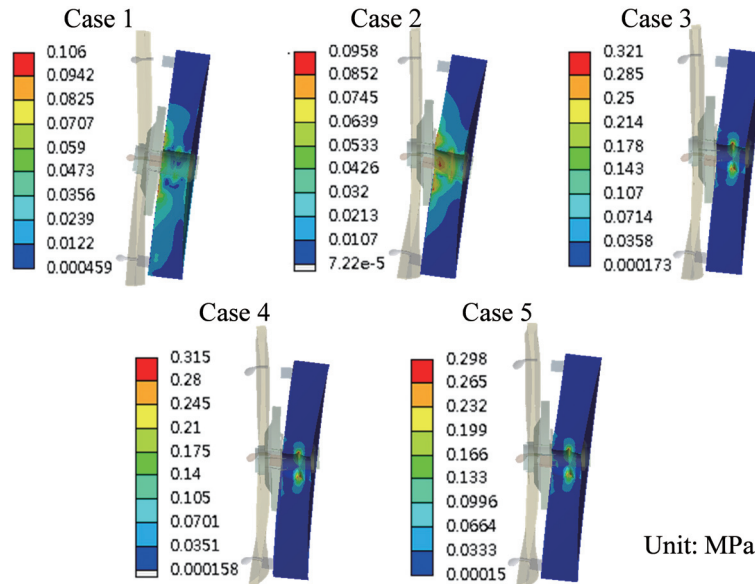


Fig. 5. Mirror stress distributions for ring support position = 35 mm. (Color online only)

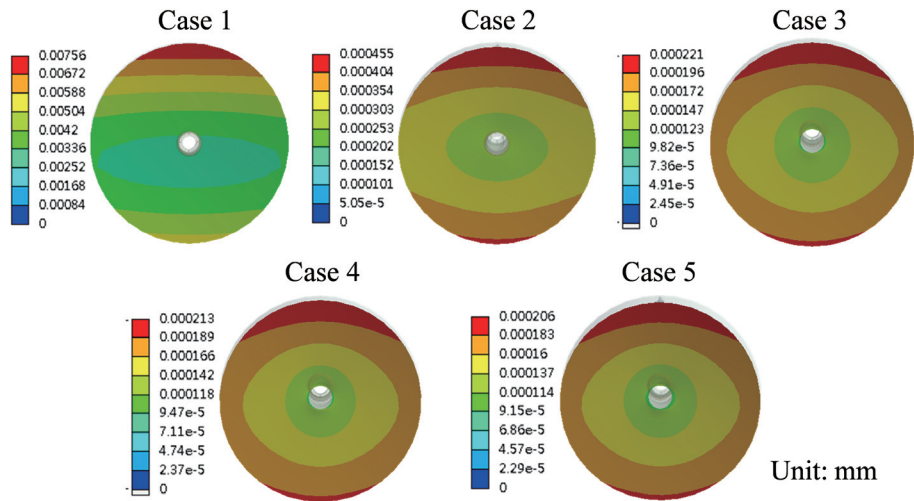


Fig. 6. Surface deformations for ring support position = 35 mm. (Color online only)

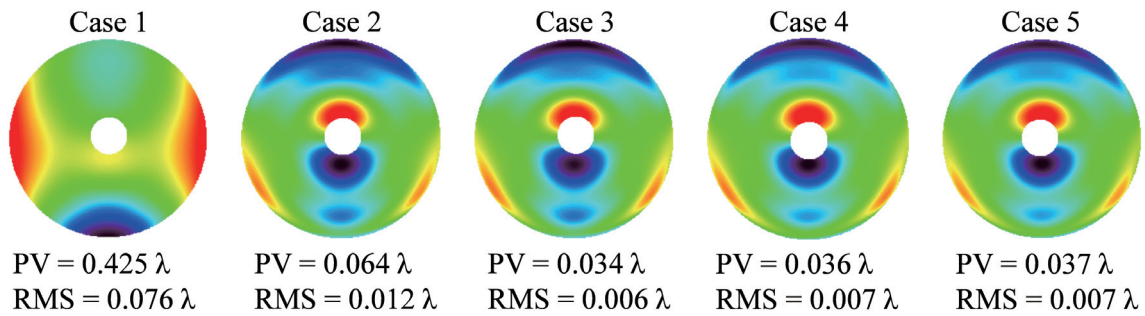


Fig. 7. OPD distributions for ring support position = 35 mm. (Color online only)

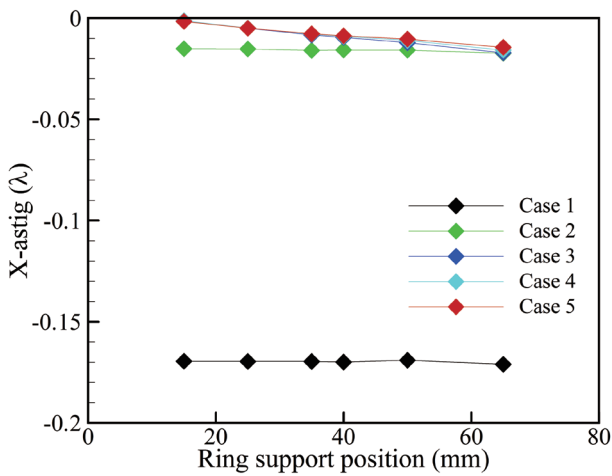


Fig. 8. The astigmatism in the X direction for five cases at various ring support positions. (Color online only)

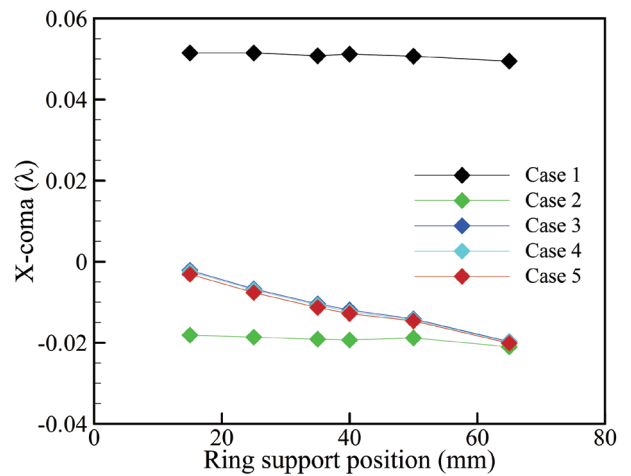


Fig. 9. The coma in the X direction for five cases at various ring support positions. (Color online only)

and coma (Fig. 9) in the X direction for Case 1 are also both much larger than those for other cases. As the ring support position is closer to the origin (the vertex of the mirror surface), the astigmatism (Fig. 8) and coma (Fig. 9) in the X direction are both slightly reduced for Cases 3 - 5.

3.2 Experimental Results

Before adjustment, the wavefront aberration configurations with and without the astigmatism in the Y direction for ring support position = 35 mm are shown in Fig. 10. For the case with the astigmatism in the Y direction (left image), the P-V and RMS wavefront errors are 0.798λ and 0.147λ respectively. This means that the collimator after integration is not in a rigid condition. The astigmatism in the X direction is 0.300λ and obviously dominates the wavefront aberration. Although the result shows inclined astigmatism configurations, the astigmatism in the Y direction actually is smaller and hence will be removed for identifying the cross arranged adjustment screw effect.

After comparing the experimental and simulation results, it was found that the OPD pattern for Case 1 is dominated by the astigmatism in the X direction and close to the experimental measurement after removing the astigmatism in the Y direction (Fig. 11). The difference between the experimental measurement (left image) and Case 1 was due to the real manufacture error and assembly errors, which were not considered in the simulations. Therefore, Case 1 with the fixed ring support position of 35 mm will be adopted for further simulations.

3.3 Adjustment Effect on the Collimator M1 Surface Deformation

Intuitively, the fine adjustment screw D should be used to push the mirror back for adjustment first because the mirror bends forward. The maximum deformations and surface aberrations for various rotation degrees using the fine adjustment screw D are shown in Fig. 12. As the rotation degree increases, the maximum deformation and astigmatism values in the X direction decrease, but the P-V and coma values in the X direction increase slightly.

Furthermore, the wavefront aberration configurations and 3D OPD maps for various rotation degrees using fine adjustment screw D are revealed in Fig. 13. The configurations for various rotation degrees are seen almost the same (Fig. 13a). The worse OPD is observed (not flat OPD) as the rotation degree increases (Fig. 13b). This is because the back of the bent mirror is subject to the reaction force (push force) from the boss between the mirror and fine adjustment screw D. The OPD on the back of the bent mirror becomes negative. Therefore, adjusting screw D will enlarge the OPD because the four fine adjustment screws provide only push motion on the mirror back.

The fine adjustment screws A and C are alternately adopted to provide push force on the left and right sides. After adjustment, the maximum stresses and deformations for various rotation degrees using the fine adjustment screws A and C are shown in Fig. 14. The maximum stresses and deformations on the mirror both increase with increasing rotation degrees. However, the P-V value reaches the minimum and the astigmatism and coma in the X direction both pass through zero for the rotation degree equal to 5, as shown in Fig. 15. The 3D OPD maps for various rotation degrees using the fine adjustment screws A and C are shown in Fig. 16. The OPD becomes flat as the rotation degree is increased to 4 and 5 degrees. However, as the rotation degree becomes 6 degrees, the OPD becomes uneven again because too much force is applied on the mirror back. It is concluded that a critical range exists for the adjustment on the collimator M1 surface deformation in spite of more induced stress and deformation.

After providing around 5 degrees of rotation to the adjusting screws C and D, the comparison of the experimental measurement before adjustment (left image) and after adjustment is shown in Fig. 17. The P-V value and the astigmatism in the X direction for the collimator M1 decrease

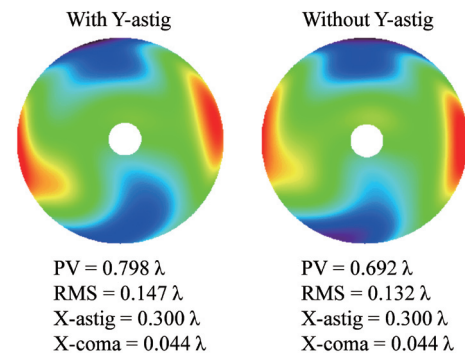


Fig. 10. Measured wavefront aberration configurations with and without the astigmatism in the Y direction for ring support position = 35 mm. (Color online only)

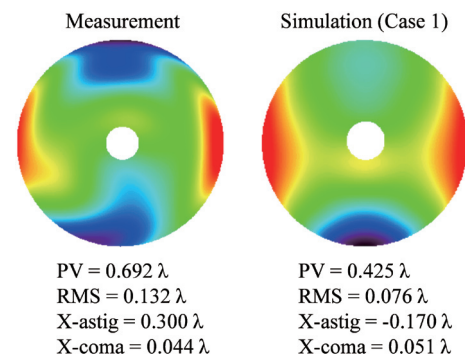


Fig. 11. Comparison of the experimental measurement (left image) and simulation result (Case 1). (Color online only)

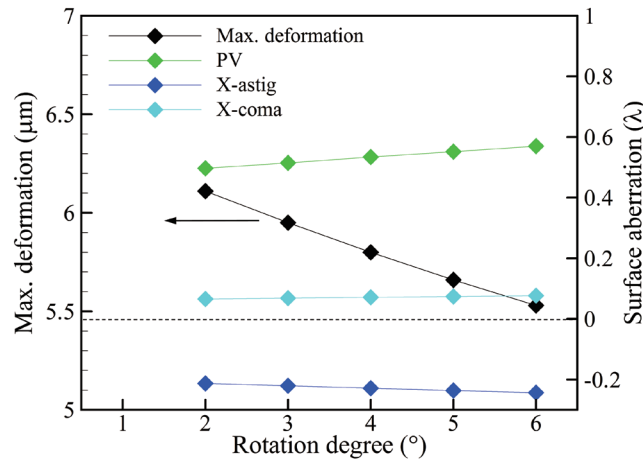


Fig. 12. Maximum deformations and surface aberrations for various rotation degrees using the fine adjustment screw D. (Color online only)

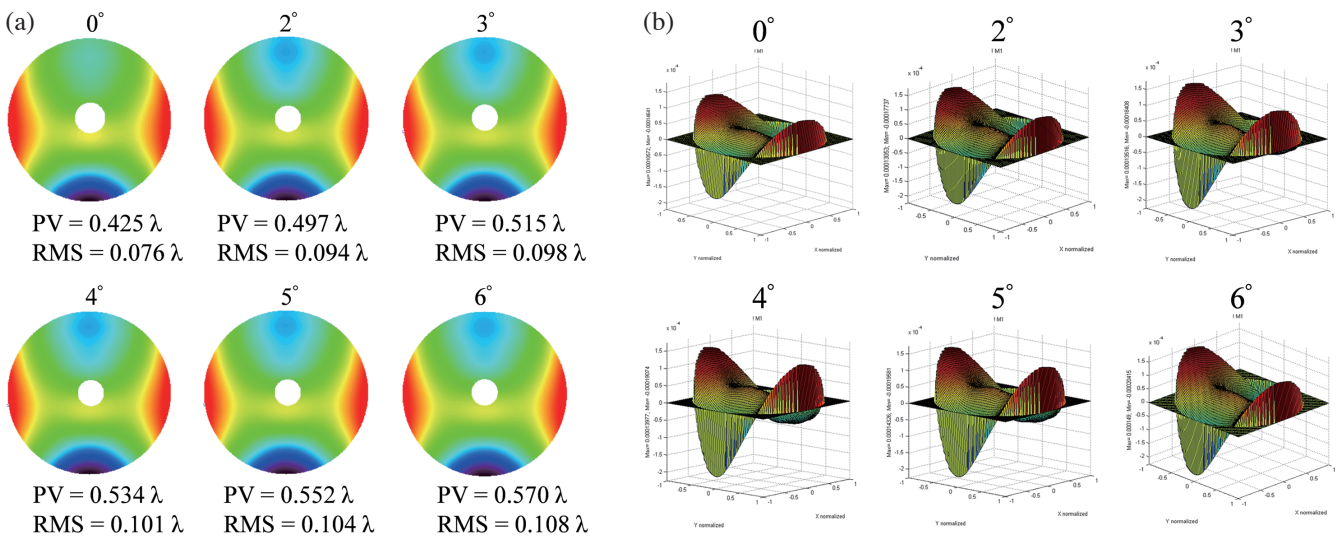


Fig. 13. (a) Wavefront aberration configurations and (b) 3D OPD map for various rotation degrees using fine adjustment screw D. (Color online only)

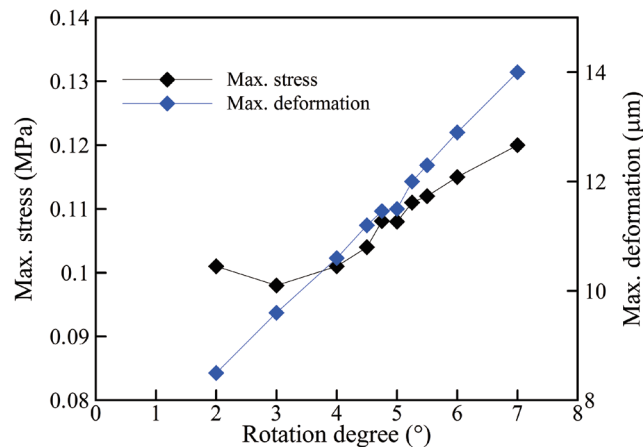


Fig. 14. Maximum stresses and deformations for various rotation degrees using fine adjustment screws A and C. (Color online only)

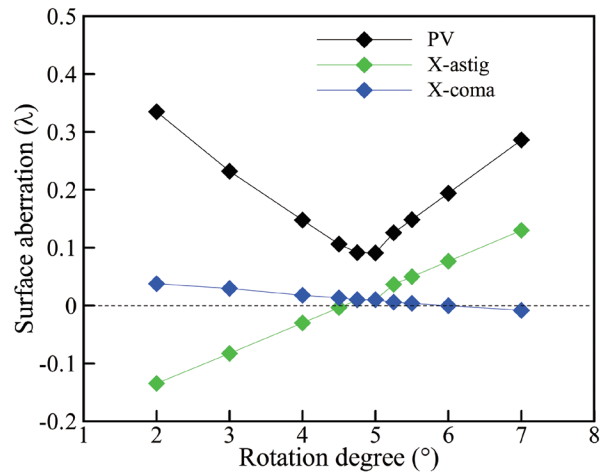


Fig. 15. Surface aberrations for various rotation degrees using fine adjustment screws A and C. (Color online only)

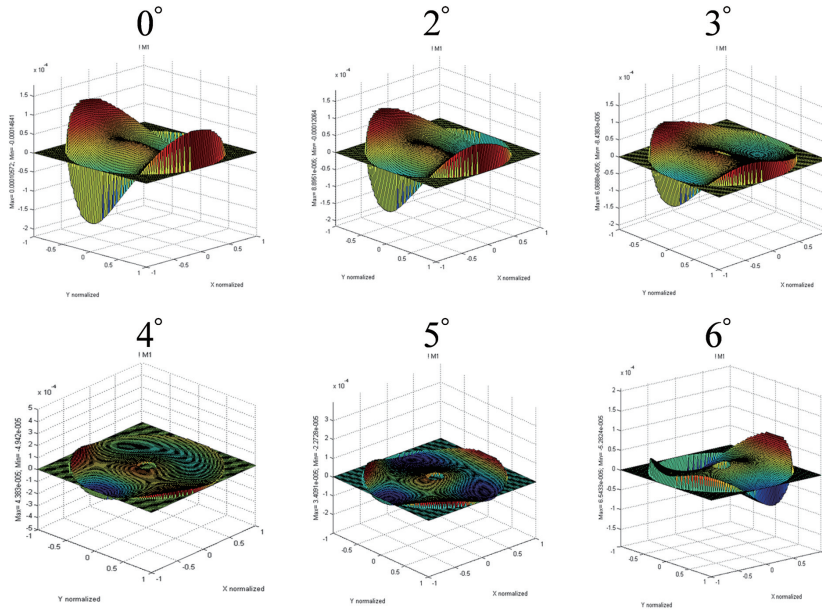


Fig. 16. 3D OPD map for various rotation degrees using fine adjustment screws A and C. (Color online only)

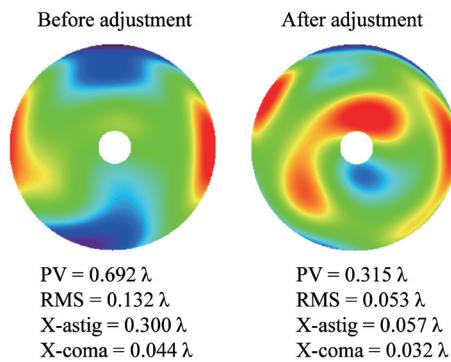


Fig. 17. Comparison of the experimental measurement before adjustment (left image) and after adjustment. (Color online only)

from 0.692λ to 0.315λ and from 0.300λ to 0.057λ , respectively, proving the correctness of the simulation results.

4. CONCLUSION

Using FEM, a ZERODUR® mirror 620 mm in diameter was analysed to obtain the deformation induced by the supporting structures. The Zernike polynomials were adopted to fit the optical surface and separate the corresponding aberrations. Through studies under different boundary conditions and supporting positions for the inner ring, it is concluded that the optical performance can be improved by choosing a suitable fixed support for the collimator structure.

The computed and measured wavefront aberration configurations for the collimator M1 were obtained complementally. The wavefront aberrations were adjusted using the fine adjustment screws with the 3D OPD map of the mirror surface. The best adjustment position was attained and applied to the actual collimator M1 to prove the correctness of the simulation results.

Acknowledgements This research was supported mainly by the Ministry of Science and Technology (MOST), National Space Organization and Instrument Technology Research Center of National Applied Research Laboratories of Taiwan, and also sponsored by the MOST Project under grant number: MOST 104-2119-M-492-008.

REFERENCES

- Beraud, P., J. Espiard, R. Geyl, J. Paseri, P. Dierickx, D. Enard, and A. Michel, 1995: Optical figuring and testing of the VLT 8.2-m primary mirrors. *Proc. SPIE*, **2536**, doi: 10.1117/12.218460. [[Link](#)]
- Chu, C., Y. Li, W. Chai, and X. Fan, 2011: Design of bipod flexures for space mirror. *Proc. SPIE*, **8196**, doi: 10.1117/12.902227. [[Link](#)]
- Döhring, T., A. Thomas, R. Jedamzik, H. Kohlmann, and P. Hartmann, 2007: Manufacturing of lightweighted ZERODUR components at SCHOTT. *Proc. SPIE*, **6666**, doi: 10.1117/12.733770. [[Link](#)]
- Kihm, H., H. S. Yang, I. K. Moon, J. H. Yeon, S. H. Lee, and Y. W. Lee, 2012: Adjustable bipod flexures for mounting mirrors in a space telescope. *Appl. Optics*, **51**, 7776-7783, doi: 10.1364/AO.51.007776. [[Link](#)]
- Li, F., P. Ruan, and B. Zhao, 2005: Study on the surface deformation of flat reflector under gravity load. *Acta Photonica Sinica*, **34**, 272-275.
- Martin, H. M., S. P. Callahan, B. Cuerden, W. B. Davison, S. T. DeRigne, L. R. Dettmann, G. Parodi, T. J. Trebisky, S. C. West, and J. T. Williams, 1998: Active supports and force optimization for the MMT primary mirror. *Proc. SPIE*, **3352**, doi: 10.1117/12.319262. [[Link](#)]
- Peng, Y. and L. Yuan, 2009: Aberration analysis for development of a large-aperture reflector by finite element. *Proc. SPIE*, **7281**, doi: 10.1117/12.831440. [[Link](#)]
- Peng, Y., Y. Dai, S. Chen, J. Wang, and Z. Zheng, 2011: High-precision figure testing of large-aperture space mirrors. *J. Appl. Optics*, **32**, 1166-1172.
- Vukobratovich, D. and R. M. Richard, 1988: Flexure mounts for high-resolution optical elements. *Proc. SPIE*, **0959**, doi: 10.1117/12.947774. [[Link](#)]
- Wu, M. Y. and Y. C. Li, 2011: Finite element analysis of large mirror based contact theory. 2011 Second International Conference on Mechanic Automation and Control Engineering (MACE), IEEE, 4964-4966, doi: 10.1109/MACE.2011.5988129. [[Link](#)]
- Wu, Q., E. Lu, J. Wang, X. Zhang, and X. Niu, 1996: Study on the surface figure changes of primary mirror centrally supported under gravity load. *Optic. Precis. Eng.*, **4**, 23-28.
- Xu, R., L. Liu, L. Zhu, and H. Liu, 2004: Support schemes and thermal effects analyses of large-aperture interferometer mirrors. *Proc. SPIE*, **5531**, doi: 10.1117/12.557956. [[Link](#)]
- Yang, H. S., M. S. Kang, S. H. Kim, Y. W. Lee, J. H. Lee, J. B. Song, H. Y. Lee, S. W. Kim, J. U. Lee, and I. W. Lee, 2005: Development of Cassegrain type 0.9-m collimator. *Proc. SPIE*, **5869**, doi: 10.1117/12.616174. [[Link](#)]
- Yao, P., X. Zhang, J. Zhang, and Y. Zhang, 2010: Performance study of a 1.2 m active mirror. *Proc. SPIE*, **7654**, doi: 10.1117/12.866876. [[Link](#)]
- Yoder, P. R., 2005: Mounting large, horizontal-axis mirrors. *Opto-Mechanical Systems Design*, Third Edition, CRC Press, 481-502, doi: 10.1201/9781420027235.ch10. [[Link](#)]
- Yoder, P. R., 2008: Techniques for mounting larger nonmetallic mirrors. *Mounting Optics in Optical Instruments*, Chapter 11, SPIE Press, Washington, 432-509, doi: 10.1117/3.785236.ch11. [[Link](#)]
- Zhao, Y., Y. Zhou, and C. Li, 2010: A support method of large aperture light weighted primary mirror manufacturing and testing. *Proc. SPIE*, **7654**, doi: 10.1117/12.866027. [[Link](#)]